

Design Optimisation of Field-Intensified Permanent Magnet Machine

Michiel H. A. Prins and Maarten J. Kamper, *Senior Member, IEEE*

Abstract—In this paper, with the application of an electric vehicle traction drive, the design optimisation of field-intensified permanent magnet machines is considered and explained. Two rotor types are considered in the design optimisation namely a simple salient-pole rotor and a rotor with internal flux barriers. The optimisation algorithm used is explained in detail and optimised machine structures are presented and discussed. Due to high torque ripple a new topology is implemented whereby the adjacent rotor poles and barriers are made asymmetric to avoid skewing the PM rotor. The FE results of the optimised machines are verified by laboratory measurements.

Index Terms—Design optimisation, permanent magnet, field-intensified, finite element, electrical machine.

ABBREVIATIONS

FI-PM	Field intensified permanent magnet
FW-IPM	Field weakening interior permanent magnet
FE	Finite element
SP	Salient pole
FB	Flux barrier

I. INTRODUCTION

The field intensified permanent magnet (FI-PM) machine is a relatively new type of electrical machine. The easiest way to realise a FI-PM machine is by adding q -axis flux barriers to obstruct the q -axis flux paths so that $L_d > L_q$, as shown in Fig. 1a. The permanent magnet (PM) is situated on the d -axis and therefore its height must not be larger than the combined height of the q -axis flux barriers in order to keep $L_d > L_q$. With $L_d > L_q$ a positive d -axis current I_d (or field-intensified current) is required rather than the classical negative I_d current for field weakening interior permanent magnet (FW-IPM) machines, as shown in Fig. 1b. This is a big advantage over classical FW-IPM machines since the positive I_d assists the PM flux instead of opposing it, therefore, reducing the risk of PM demagnetisation. Therefore thinner magnets can be used, thus reducing cost. Initially the FI-PM machine operates with positive I_d to benefit from the reluctance torque. As the speed increases and the voltage limit is reached, the positive I_d needs to be reduced by advancing the current space phasor angle so that I_d eventually becomes negative (FW current) to prevent the voltage increasing with speed. Only a small amount of negative I_d is needed above rated speed to obtain good FW capabilities [1]. Another advantage of FI-PM machines is that the saliency does not disappear under increasing load conditions i.e with increasing I_q current. This can be explained by the q -axis flux paths which saturate

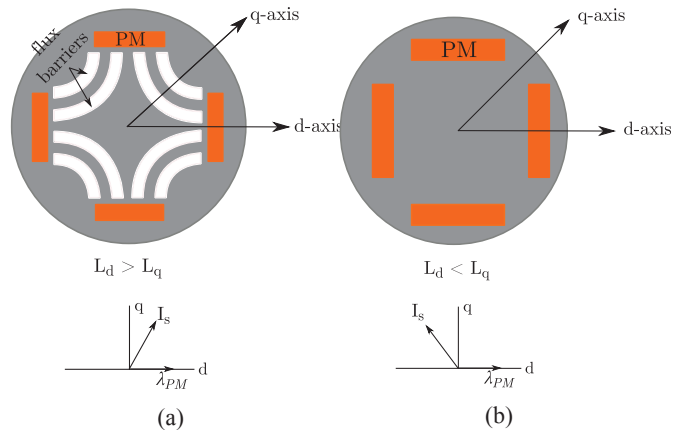


Fig. 1: (a) FI-PM machine topology. (b) FW-IPM machine topology.

as I_q increases with load, which causes L_q to decrease. Due to $L_d > L_q$ the difference between the two inductances becomes larger as the load increases, thus, causing the saliency to increase. The saliency is much more linear, due to fewer saturation effects, than in FW-IPM machines, which is advantageous for sensorless control [1].

The first FI-PM machine was introduced in 1999 by [2] who added flux barriers in the rotor to obstruct q -axis flux paths so that $L_d > L_q$. This was done to achieve higher torque capabilities above rated speed i.e. in the FW operating region. In 2006 the main focus was to design a cost effective machine but still to maintain a high power density, hence, a machine with low PM volume [3].

In 2009 a FI-PM machine was designed by [4] to improve the sensorless capabilities of the machine especially at low speed [4]. In 2010 a study of FI-PM machines with distributed and concentrated windings was conducted [5]. The effects of the two winding configurations on the sensorless control performance were investigated.

A new rotor design was proposed by [1] for a FI-PM machine that is more suitable for sensorless control at zero/very-low speed. In 2012 the focus of [6], [7] was to reduce expensive rare earth materials even more by using low coercive force magnets with magnetisation level control. In 2013 the sensorless control capability of a FI-PM machine was investigated using several sensorless control methods. The FI-PM machine showed good sensorless capabilities with good estimation accuracy for all the methods [8].

Despite all the literature hitherto on FI-PM machines no work has been published on the design optimisation of FI-PM machines. Therefore in this paper the design optimisation of FI-PM machines for an electric vehicle drive application is explained.

II. DESIGN SPECIFICATIONS

FI-PM machines are designed and optimised for a multi-gear electric vehicle application. The design specifications are according to the tractive effort and power

Michiel H. A. Prins and Maarten J. Kamper are with the Department of Electrical and Electronic Engineering, Stellenbosch University, Stellenbosch, South Africa, phone: +27(0)21-808-4323; fax: +27(0)21-808-3951; e-mail: kamper@sun.ac.za.

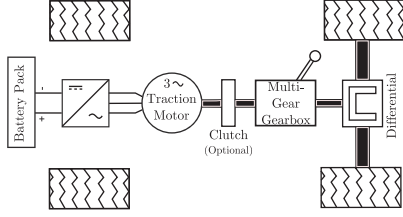


Fig. 2: Multiple-gear with differential drive.

TABLE I: Design specifications of electric traction motor

Parameter	Value	Unit
Rated torque	70	Nm
Rated power	35	kW
Rated speed	4800	r/min
Battery pack voltage	350	V DC
Max. stator outer diameter	230	mm
Shaft diameter	43	mm
Max. stack length	110	mm
Min. air-gap length	0.4	mm
Number of poles	4	
Cooling	air	

specification of a internal combustion engine powered Opel Corsa. The standard clutch and 5-speed manual transmission with differential of the Opel Corsa are used for the investigation. With a multi-gear drive FW is not necessary. In this case, thus, the FW performance of the FI-PM machine is not important in the design optimisation. A multi-gear plus differential electric drive-train setup is shown in Fig. 2. The traction motor design specifications calculated from the tractive effort and power specifications are given in Table I.

III. STEADY-STATE MACHINE MODEL

The equivalent dq parameters used in the design optimisation are shown in Fig. 3. The steady-state dq voltages are calculated by

$$V_d = I_d r_s - \omega_e (\lambda_q + \lambda_{eq}) \quad \text{and} \quad (1)$$

$$V_q = I_q r_s + \omega_e (\lambda_d + \lambda_{ed} + \lambda_{PM}), \quad (2)$$

where r_s is the stator winding resistance and ω_e the electrical rotor angular velocity. The dq flux linkages, λ_d and λ_q , include the leakage flux linkage λ_l and the fundamental stator winding air-gap flux linkage λ_g .

The dq voltage equations also include the end-winding flux leakage speed voltages calculated from the end-winding leakage inductance. An approximate end-winding leakage inductance formula of [9] is used as

$$L_e = 4.55 \times 10^{-7} d_{si} W^2, \quad (3)$$

where d_{si} is the stator bore inner diameter and W the amount of turns in series per phase. From (3) the end-winding leakage flux linkage is calculated for the d - and q -axis by

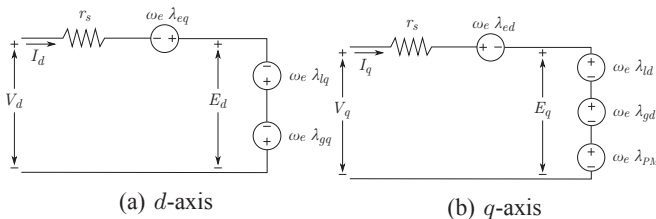


Fig. 3: Steady-state d - and q -axis equivalent circuits of the FI-PM machine.

$$\lambda_{ed} = L_e I_d \quad \text{and} \quad (4)$$

$$\lambda_{eq} = L_e I_q \quad (5)$$

respectively. The current space phasor is defined by $\mathbf{I}_s = I \angle \phi = I_d + j I_q$ where ϕ is the current space phasor angle. The electromagnetic torque is calculated in the design optimisation as a function of the magnitude and angle of the current space phasor ϕ by

$$T_{em} = \frac{3}{4} p (L_d - L_q) I_s^2 \sin(2\phi) + \frac{3}{2} p \lambda_{PM} I_s \sin(\phi), \quad (6)$$

In (6) the term $L_d - L_q$ is the saliency where L_d and L_q are the d - and q -axis stator inductances. These dq inductances are defined by

$$L_d = \frac{\lambda_d}{i_d} \quad \text{and} \quad (7)$$

$$L_q = \frac{\lambda_q}{i_q} \quad (8)$$

respectively. From the instantaneous and average torques the % peak-to-peak torque ripple used in the design optimisation is calculated by

$$T_{rip} = \left(\frac{T_{max} - T_{min}}{T_{avg}} \right) 100\%. \quad (9)$$

Since the copper losses are dominant in the relatively small motor considered in this paper, the efficiency is greatly affected by it. The copper loss is calculated by

$$P_{cu} = \frac{3}{2} I_s^2 r_s. \quad (10)$$

IV. FE DESIGN OPTIMISATION

The design optimisation of the FI-PM machines is done by means of optimisation algorithms of the VisualDoc software [10] together with Python scripts and the JMAG finite element (FE) simulation software. The optimisation is an iterative process where the optimisation algorithms repeatedly call the FE software, by means of the Python scripts, to calculate the objective function and other performance parameters. The optimisation algorithms used are gradient-based algorithms for constrained problems which make use of line search methods.

A. FI-PM machine optimisation

The optimum design of two FI-PM machines is considered in this paper. The first FI-PM machine has a salient-pole (SP) rotor structure with only a few design variables as shown in Fig. 4a. The stator of this machine is not optimised as a stator of a previously designed and manufactured machine for the Corsa EV drive (for the same specifications) is used for testing purposes. Hence, the active stack length in this case is fixed. The second FI-PM machine has a more complex rotor structure with internal flux barriers (FBs) as shown in Fig. 4b.

The objective function in the optimisation of the SP FI-PM machine is to minimise the PM volume subject to a specification constraint, since it contains expensive rare earth materials, thereby, reducing cost. By reducing the PM

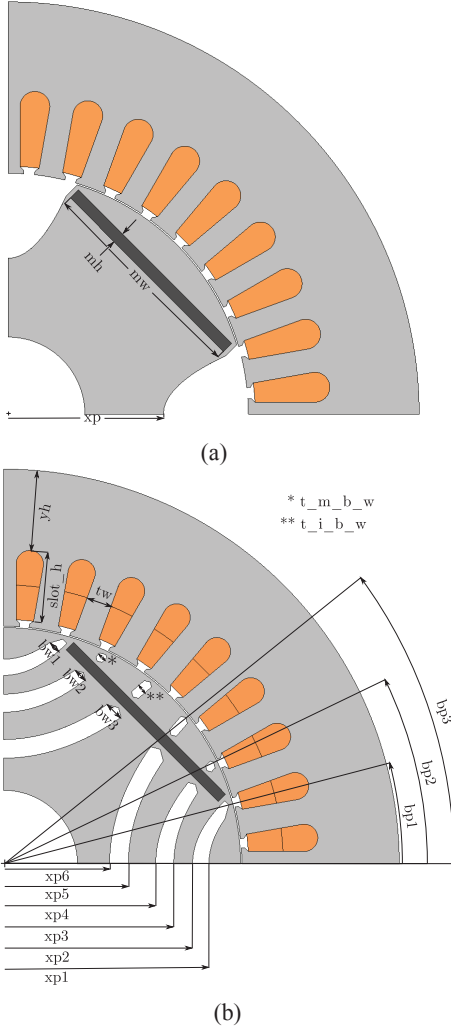


Fig. 4: Quarter cross-section showing the rotor design variables of (a) the SP FI-PM machine and (b) the FB FI-PM machine.

volume the PM thickness will reduce, which will cause the d -axis inductance L_d to increase, which is favourable for FI-PM machines. The PM thickness can be reduced with minimised risk of PM demagnetisation [11]. Note that the PM in the SP-rotor is located to its left and right between small iron bridges of 1.1 mm as shown in Fig. 4a. Therefore, as the PM width changes in the design optimisation, the pole width also changes accordingly.

The other parameters of the equivalent circuits used in the design optimisation are calculated from the rated dq currents and rated current density (8.5 A/mm^2). The objective function to be minimised is expressed as

$$F(\mathbf{X}) = V_{PM}(\mathbf{X}) \quad (11)$$

subject to the constraint of

$$\mathbf{g} = [T_{avg}] > [70.0] \text{ (Nm)} \quad (12)$$

and constants as

$$\mathbf{u} = \begin{bmatrix} ro_{od} \\ ro_{id} \\ \ell_s \end{bmatrix} = \begin{bmatrix} 133.6 \text{ mm} \\ 43.0 \text{ mm} \\ 110.0 \text{ mm} \end{bmatrix}, \quad (13)$$

where ro_{od} is rotor outer diameter, ro_{id} is rotor shaft diameter and ℓ_s is axial stack length. The matrix vector \mathbf{X} of (11) includes design variables as explained in Fig. 4a as

TABLE II: Optimum design variables obtained from the optimisation for the SP FI-PM machine.

Variables	ϕ	x_p	m_w	m_h
Values	71.0°	43.45 mm	60.64 mm	3.0 mm

$$\mathbf{X}^T = [\phi \quad x_p \quad m_w \quad m_h]. \quad (14)$$

Since the torque is a function of the current space phasor angle ϕ as given in (6), it is a variable in the design optimisation as given in (14), to ensure the optimum angle for maximum torque minimising the PM volume. The optimum PM thickness or height, m_h , found from the optimisation was 2.0 mm, but due to the fragility of the PM and manufacturing constraints, the height was specified by the manufacturers not to be less than 3 mm. The optimum values for the design variables obtained from the optimisation are given in Table II. From the PM height m_h , PM width m_w and stack length $\ell_s=100 \text{ mm}$ the PM volume of the machine is determined to be 80.05 cm^3 .

The rotor structure of the FB FI-PM machine to be optimised consists of flux barriers across the q -axis flux paths in order to reduce the q -axis inductance L_q and cause $L_d > L_q$. The FB FI-PM machine has a lot more design variables than the SP FI-PM machine due to its complex rotor structure and the stator which is also optimised. The stator has three design variables while the rotor has fourteen design variables as shown in Fig. 4b. In the optimisation of the SP FI-PM machine it was observed that the PM height m_h decreased to a value below the allowed minimum. Therefore the PM height is fixed in the FB FI-PM machine design optimisation to a minimum of 3 mm. The PM width m_w is fixed between small 1.1 mm iron bridges to the tips of the outer flux barrier, therefore as the pitch of the outer barrier changes in the design optimisation, the PM width changes accordingly as is clear from Fig. 4b. The pitch of the flux barriers is an important design parameter as the torque ripple is greatly influenced by the position of the tips of the flux barriers [12]. The iron ribs in the rotor have a thickness of 1.1 mm to prevent mechanical failure at maximum speed.

The objective function is to minimise the $\frac{P_{cu}}{T_{avg}}$. Since the major part of the losses in this machine comprise of copper loss [13], minimising $\frac{P_{cu}}{T_{avg}}$ is close to maximising the efficiency of the machine; including the small part of iron losses in the design optimisation of this relatively small sized machine will have little effect on the optimum design values. The current density J in the optimisation is kept at 8.5 A/mm^2 . As the minimisation is subject to a torque constraint, the objective function to be minimised is expressed as

$$F(\mathbf{X}) = P_{cu}(\mathbf{X}) \quad (15)$$

subject to the constraints of

$$\mathbf{g} = \begin{bmatrix} 70.0 \\ 0.0 \end{bmatrix} < \begin{bmatrix} T_{avg} \\ T_{rip} \end{bmatrix} < \begin{bmatrix} - \\ 20.0 \end{bmatrix} \begin{matrix} \text{(Nm)} \\ \text{(\%)} \end{matrix} \quad (16)$$

and constants as

$$\mathbf{u} = \begin{bmatrix} st_{od} \\ ro_{id} \\ \ell_g \end{bmatrix} = \begin{bmatrix} 230.0 \text{ mm} \\ 43.0 \text{ mm} \\ 0.4 \text{ mm} \end{bmatrix}, \quad (17)$$

where the matrix vector \mathbf{X} includes the 19 design variables

TABLE III: Optimum design values of the FB-rotor FI-PM machine of Fig. 4b.

Var	Values	Var	Values	Var	Values
ϕ	84.24 °	x_{p2}	54.94 mm	bw_1	3.63 mm
ℓ_s	89.9 mm	x_{p3}	49.47 mm	bw_2	4.1 mm
y_h	23.35 mm	x_{p4}	44.22 mm	bw_3	5.53 mm
$slot_h$	22.38 mm	x_{p5}	36.28 mm		
t_w	7.34 mm	x_{p6}	30.83 mm		
t_{i_bw}	2.78 mm	bp_1	15.29 °		
t_{m_bw}	2.39 mm	bp_2	25.98 °		
x_{p1}	59.68 mm	bp_3	38.89 °		

as partly shown in Fig. 4b as

$$\mathbf{X}^T = \begin{bmatrix} \phi & \ell_s & y_h & slot_h & t_w & \dots \\ \dots & t_{i_bw} & t_{m_bw} & x_{p1} & x_{p2} & \dots \\ \dots & x_{p3} & x_{p4} & x_{p5} & x_{p6} & \dots \\ \dots & bp_1 & bp_2 & bp_3 & bw_1 & \dots \\ \dots & bw_2 & bw_3 & & & \dots \end{bmatrix}. \quad (18)$$

The current space phasor angle ϕ is again a variable in the design optimisation. Also the stack length ℓ_s in this case is a variable to ensure a minimum length for the FB FI-PM machine.

The optimum values for the design variables are given in Table III. Note the 18.27 % decrease in ℓ_s from the SP FI-PM machine. The decrease in ℓ_s is due to the flux barriers in the rotor which generate more reluctance torque than the SP FI-PM machine. The PM volume decreased by 15.74 % to 67.45 cm³.

B. Torque ripple minimisation

The SP FI-PM and FB FI-PM machines exhibit a high torque ripple which can be reduced by skewing the rotor by means of a number of stacks. Due to the PMs it is difficult to skew the machine in the manufacturing process. Hence, a relatively new topology is implemented where the adjacent poles of the machine, or the flux barriers in the adjacent poles, are asymmetric. This topology was first introduced in 2004 by [12]. Several other authors also investigated asymmetric flux barrier arrangements which include [14]–[16]. One drawback of this topology is that two poles of the machine need to be modelled in order for the boundary conditions to match in the FE analysis. This increases the FE design optimisation time.

The rotor structure of the optimised SP FI-PM motor causes a high torque ripple of 39%. An optimisation with asymmetric poles was conducted where the objective function was to minimise the torque ripple with only the magnet (or pole) widths as variables as shown in Fig. 5. The objective function to be minimised is

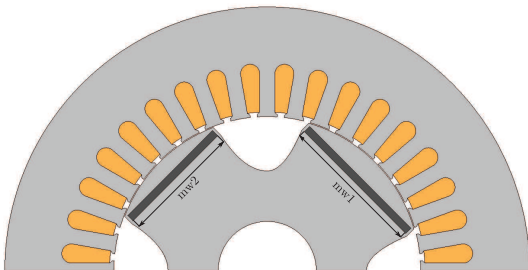


Fig. 5: Half cross-section showing the design variables of the asymmetric SP FI-PM machine.

TABLE IV: Optimum PM widths found from the optimisation for the asymmetric SP FI-PM machine.

Variables	mw_1	mw_2
Values	62.78 mm	52.5 mm

TABLE V: Optimum flux barrier pitches found from the optimisation for the asymmetric FB FI-PM machine.

Variables	Values	Variables	Values
bp_1	10.01 °	bp_4	14.05 °
bp_2	18.88 °	bp_5	25.24 °
bp_3	31.24 °	bp_6	38.01 °

$$F(\mathbf{X}) = T_{rip}(\mathbf{X}) \quad (19)$$

subject to the constraint of

$$\mathbf{g} = [T_{avg}] > [70.0] (Nm), \quad (20)$$

where the matrix vector \mathbf{X} includes the optimisation variables as

$$\mathbf{X}^T = [mw_1 \quad mw_2]. \quad (21)$$

Note that in this case the other design variables in (14) are constants.

The optimum values found from the optimisation for the design variables are given in Table IV. Note the asymmetry in the pole widths as shown in Fig. 5, which causes the torque ripple to decrease to 6.6%. Note that due to (20) the torque is still according to specification.

Although the FB FI-PM machine's torque ripple is much lower than that of the SP FI-PM machine, it is still fairly high. Therefore an asymmetric flux barrier configuration was optimised where the flux barriers of the adjacent poles are asymmetric. The objective function and inequality constraint are the same as for the asymmetric SP FI-PM. The design variables to be optimised in this case are the barrier pitches as shown in Fig. 6. All the other design variables in (18) are thus constants. The vector matrix containing the design variables is given by

$$\mathbf{X}^T = [bp_1 \quad bp_2 \quad bp_3 \quad bp_4 \quad bp_5 \quad bp_6]. \quad (22)$$

The optimum values found from the optimisation for the design variables are given in Table V. Note the asymmetry in the adjacent flux barrier pitches. The asymmetry caused the torque ripple to decrease to 6.9%.

V. PM DEMAGNETISATION AND ROTOR DEFORMATION

In this section the PM demagnetisation and rotor deformation of the optimum designed FB FI-PM machine are investigated using the JMAG FE software.

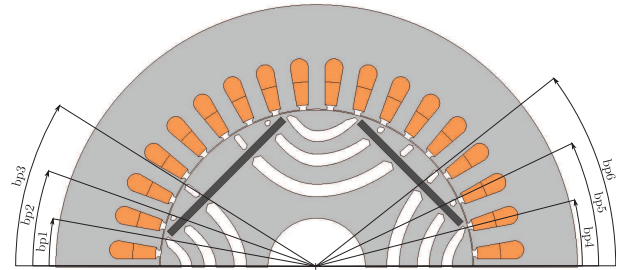


Fig. 6: Half cross-section showing the design variables of the asymmetric FB FI-PM machine.

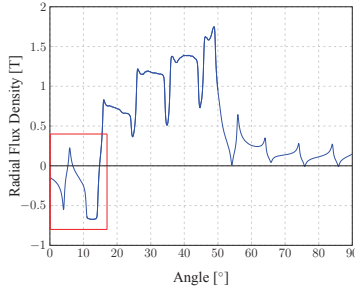


Fig. 7: Armature reaction effect on the air gap flux density of the SP FI-PM machine.

TABLE VI: Conditions investigating PM demagnetisation

Parameter	FB FI-PM
I_s (p.u.)	1.7 $\angle 84.24^\circ$
PM Temperature	120 $^\circ C$

A. Demagnetisation

All PM's are vulnerable to demagnetisation caused by temperature rise, high negative d -axis current and armature reaction effect. Although high negative d -axis current is not present due to the FI operation, careful attention must still be paid to demagnetisation due to armature reaction. The armature reaction effect is explained in Fig. 7 for the SP FI-PM machine, which shows the radial air gap flux density over a quarter of the machine at instants of current and rotor position. It can be seen that negative flux is present over some part of the PM as indicated by the red rectangle, which introduces a risk of demagnetisation if the PM is too thin.

PM demagnetisation risk studies are conducted under worst case scenario conditions for the FB FI-PM as given in Table VI. In Fig. 8a the result of the PM demagnetisation studies conducted on the FB FI-PM machine is shown. From the figure it is evident that no signs of demagnetisation is visible on the PM surface of the machine. With the temperature at 120 $^\circ C$, the current magnitude is further increased to determine at which magnitude the PMs starts to show signs of demagnetisation. It was found that the PM of the FB FI-PM machine only starts to demagnetise at a current magnitude of 390 A (2.95 p.u.) shown by the cut-out section of the machine in Fig. 8b.

B. Rotor Deformation

A centrifugal force study is done on the FB FI-PM machine to see whether rotor deformation occurs. From this study the FB rotor shows a radial displacement of 13 μm at a speed of 4800 r/min. The air-gap is 0.4 mm and therefore

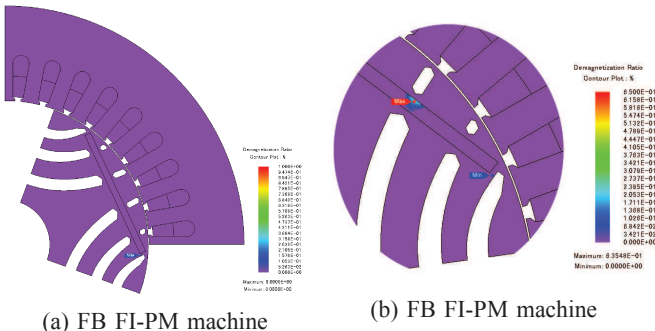


Fig. 8: Demagnetisation study of the FB FI-PM machine: (a) Quarter cross-section showing the demagnetisation ratio for the conditions in Table VI and (b) cut-out section showing signs of demagnetisation on the surface of the PM for the FB FI-PM machine at 2.95 p.u. current.

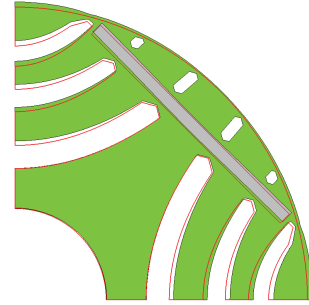


Fig. 9: Quarter cross-section of the FB FI-PM machine's rotor showing the deformation scaled by one hundred, at 4800 r/min speed.

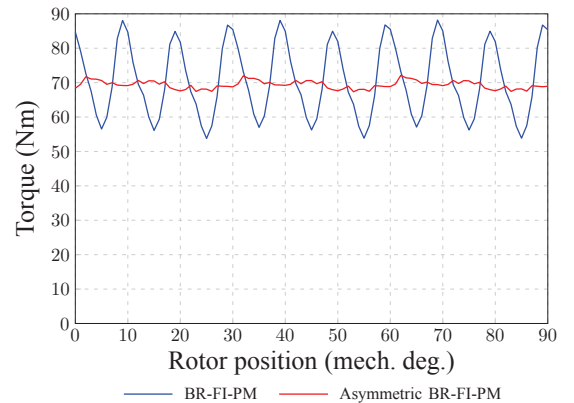
the displacement is deemed acceptable. The deformation is shown in Fig. 9 with the displacement enlarged by a factor of one hundred.

VI. FE AND MEASURED RESULTS

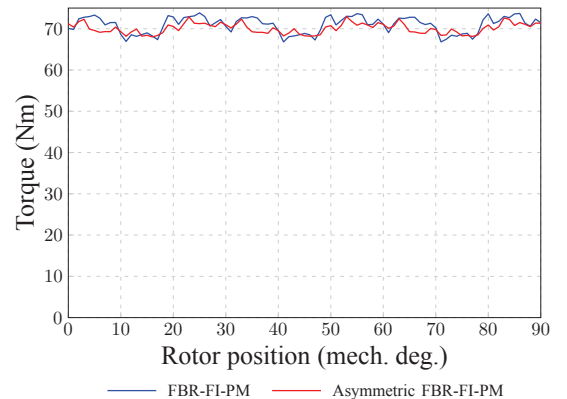
The FE calculated performance results at rated current density of each machine are given in Table VII. The performance of all the machines succeed in the design specifications as given in Table I.

It can be seen from Table VII that for the same average torque of 70 Nm, the current and voltage of the FB FI-PM machines are lower than those of the SP FI-PM machines, i.e at the same current density and turns per slot. This is due to the higher saliency and larger active rotor surface of the FB-rotor machines.

Also note how the asymmetries in the adjacent poles and barriers reduce the torque ripple. The torque waveforms of the symmetric and asymmetric rotors are compared in Figs. 10a and 10b for the SP FI-PM and FB FI-PM machines



(a) SP FI-PM machine



(b) FB FI-PM machine

Fig. 10: Torque versus rotor position of the FI-PM machines at full load.

TABLE VII: FE calculated rated performance results of the optimised machines.

	SP FI-PM	Asym. SP FI-PM	FB FI-PM	Asym. FB FI-PM
Current ($A_{\text{rms phase}}$)	142.78	142.78	132.11	132.11
Current density (A/mm^2)	8.4	8.4	8.4	8.4
Current angle (ϕ)	71	71	84.24	84.24
Voltage ($V_{\text{rms phase}}$)	123.48	119.79	108.61	110.24
Speed (r/min)	4800	4800	4800	4800
Torque (Nm)	71.53	69.36	71.06	70.1
Torque ripple (%)	39	6.6	10	6.9
Output power (kW)	35.57	34.86	35.66	35.23
Iron loss (W)	434.32	416.06	364.22	381.4
Copper loss (kW)	1.27	1.27	1.13	1.13
Efficiency (%)	95.4	95.39	95.99	95.9
Power Factor	0.7	0.71	0.86	0.83
Rotor OD (mm)	133.6	133.6	137.75	137.75

respectively. From these results an impressive torque ripple reduction is clear for the SP FI-PM machine with asymmetric poles, while the FB FI-PM machine with asymmetric flux barriers also show a good reduction in torque ripple.

In order to validate the results obtained from the



(a) Rotor (b) Stator
Fig. 11: Photos of the SP FI-PM rotor and stator.

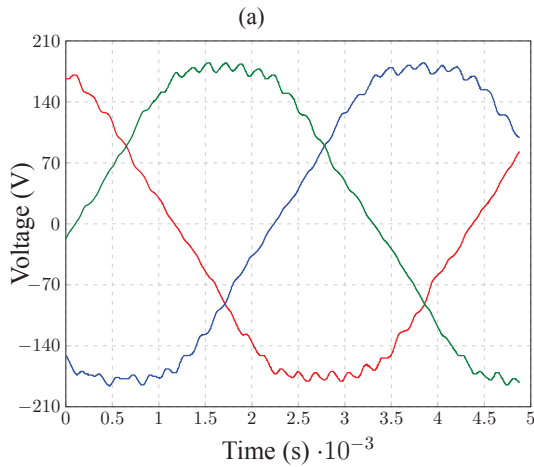
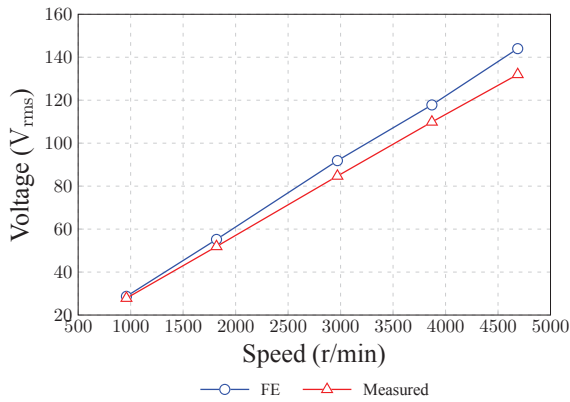


Fig. 12: (a) Measured and calculated open-circuit rms phase voltage; (b) measured open-circuit phase voltage waveforms at 156.25 Hz (4687.5 r/min) of the SP FI-PM machine.

FE models, tests were conducted in the laboratory on the asymmetric SP FI-PM machine. Figures 11a and 11b show the rotor and stator of the machine under test.

The open-circuit voltage of the SP FI-PM machine is measured by driving it with another machine at different speeds. The measurements were done up to a speed of 4800 r/min, which is equal to a vehicle speed of 126 km/h in 5th gear. The open-circuit FE calculated results were done afterwards at the measured speeds. As shown in Fig. 12a the measured results are slightly lower than the calculated FE results. This is due to the the manufacturing tolerances of the PMs. Otherwise, the measured and calculated results show good correlation. The open-circuit voltage waveform shown in Fig. 12b is the result of a measurement at 4688 r/min.

The asymmetric SP FI-PM machine was tested under steady state load conditions at several load and speed points. The results of these tests are shown in Fig. 13, with the round and filled markers the measured values and the solid lines the FE calculated values. The measured and FE calculated torques show good correlation. Note that measurements at high speed and load torque could not be done due to severe mechanical vibration of the test bench at certain speeds.

VII. CONCLUSIONS

From the analysis and results the following conclusions are drawn:

- The salient pole rotor FI-PM machine is designed with the focus to reduce the volume of the expensive

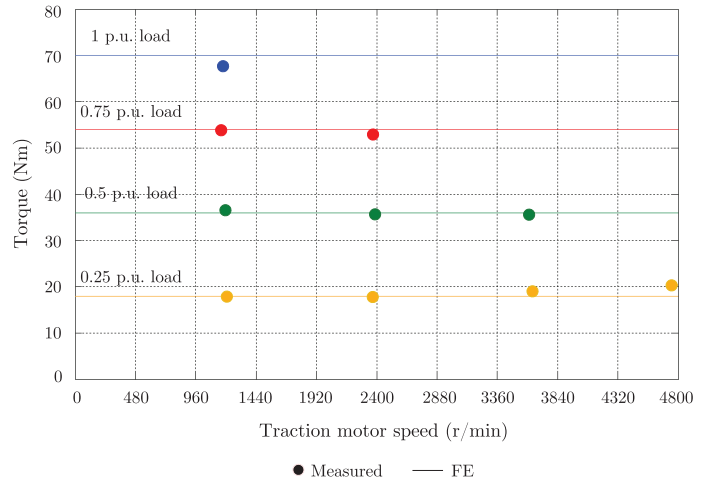


Fig. 13: Measured and FE calculated torque of SP FI-PM machine.

PM material. In this optimisation it is found that the PM height (thickness) is reduced by the optimisation algorithm beyond manufacturing capabilities, therefore it needs to be kept at a minimum height.

- The internal flux barrier rotor FI-PM machine is designed with the aim to reduce copper loss subject to a torque constraint. As the FB FI-PM machine generates more reluctance torque than the SP FI-PM machine, the stack length is decreased by the optimisation algorithm by 15.7 % and the PM volume by 15.3% of that of the SP FI-PM machine.
- It is found that both the SP FI-PM and FB FI-PM machines exhibit high torque ripple, however a topology is implemented whereby adjacent rotor poles and barriers are asymmetric to reduce torque ripple. The asymmetric layout proved to be effective for torque ripple reduction below 7% and it is thus shown that it can be used as an alternative for rotor stack skewing.
- For the EV drive application the open-circuit tests conducted showed that the back-EMF is below the allowed maximum voltage.
- The load tests conducted correlate well with the FE calculated results, therefore the FE simulations are deemed accurate.

REFERENCES

[1] N. Limsuwan, Y. Shibukawa, D. Reigosa, and R. Lorenz, "Novel design of flux-intensifying interior permanent magnet synchronous machine suitable for self-sensing control at very low speed and power conversion," *IEEE Transactions on Industry Applications*, vol. 47, no. 5, pp. 2004–2012, Sept.-Oct. 2011.

[2] N. Bianchi and S. Bolognani, "Performance analysis of an ipm motor with segmented rotor for flux-weakening applications," in *Ninth International Conference on Electrical Machines and Drives, 1999. (Conf. Publ. No. 468)*, 1999, pp. 49–53.

[3] A. Akatsu, M. Arimitsu, and S. Wakui, "Design and control of field intensified interior permanent magnet synchronous machine," *IEEE Transactions on Industry Applications*, vol. 126, no. 7, pp. 827–834, 2006.

[4] S. Wu, D. Reigosa, Y. Shibukawa, M. Leetmaa, R. Lorenz, and Y. Li, "Interior permanent-magnet synchronous motor design for improving self-sensing performance at very low speed," *IEEE Transactions on Industry Applications*, vol. 45, no. 6, pp. 1939–1946, Nov.-Dec. 2009.

[5] D. Reigosa, K. Akatsu, N. Limsuwan, Y. Shibukawa, and R. Lorenz, "Self-sensing comparison of fractional slot pitch winding versus distributed winding for fw- and fi-ipmsms based on carrier signal injection at very low speed," *IEEE Transactions on Industry Applications*, vol. 46, no. 6, pp. 2467–2474, 2010.

[6] T. Kato, N. Limsuwan, C. Yu, K. Akatsu, and R. Lorenz, "Rare earth reduction using a novel variable magnetomotive force, flux intensified ipm machine," in *Energy Conversion Congress and Exposition (ECCE), 2012 IEEE*, 2012, pp. 4346–4353.

[7] N. Limsuwan, T. Kato, K. Akatsu, and R. Lorenz, "Design and evaluation of a variable-flux flux-intensifying interior permanent magnet

machine," in *Energy Conversion Congress and Exposition (ECCE), 2012 IEEE*, 2012, pp. 3670–3677.

[8] C.-Y. Yu, J. Tamura, D. Reigosa, and R. Lorenz, "Position self-sensing evaluation of a fi-ipmsm based on high-frequency signal injection methods," *IEEE Transactions on Industry Applications*, vol. 49, no. 2, pp. 880–888, 2013.

[9] M. Kamper and F. Van der Merwe, "Design optimisation of cageless flux barrier rotor reluctance synchronous machine," Ph.D. dissertation, University of Stellenbosch, December 1996.

[10] G. Vanderplaats, *Numerical Optimization Techniques for Engineering Design*, 4th ed., V. Research and D. Incorporation, Eds. Mcgraw Hill, 2005.

[11] R. Lorenz, N. Limsuwan, Y. Shibukawa, and D. Reigosa, "Novel design of flux-intensifying interior permanent magnet synchronous machine suitable for self-sensing control at very low speed and power conversion," *IEEE Transactions on Industry Applications*, vol. 47, no. 5, pp. 2004–2012, 2011.

[12] M. Sanada, K. Hiramoto, S. Morimoto, and Y. Takeda, "Torque ripple improvement for synchronous reluctance motor using an asymmetric flux barrier arrangement," *IEEE Transactions on Industry Applications*, vol. 40, no. 4, pp. 1076–1082, 2004.

[13] M. H. Prins, C. W. Vorster, and M. J. Kamper, "Reluctance synchronous and field intensified-pm motors for variable-gear electric vehicle drives," in *Energy Conversion Congress and Exposition (ECCE), 2013 IEEE*, 2013, pp. 657–664.

[14] N. Bianchi, S. Bolognani, D. Bon, and M. Pre, "Rotor flux-barrier design for torque ripple reduction in synchronous reluctance and pm-assisted synchronous reluctance motors," *IEEE Transactions on Industry Applications*, vol. 45, no. 3, pp. 921–928, 2009.

[15] P. Alotto, M. Barcaro, N. Bianchi, and M. Guarnieri, "Optimization of interior pm motors with machaon rotor flux barriers," *IEEE Transactions on Magnetics*, vol. 47, no. 5, pp. 958–961, 2011.

[16] L. Alberti, M. Barcaro, and N. Bianchi, "Design of a low torque ripple fractional-slot interior permanent magnet motor," in *Energy Conversion Congress and Exposition (ECCE), 2012 IEEE*, 2012, pp. 509–516.

VIII. BIOGRAPHIES

Michiel H.A. Prins (S'11) was born in Paarl, South Africa, in November 1986. He received the B.Tech. and M.Tech degrees in electrical and electronic engineering in 2009 and 2011, respectively, from the Cape Peninsula University of Technology, Cape Town, South Africa. He was employed by Optimal Energy where he took part in the electric traction motor design for the Joule Electric Vehicle. He received the M.Sc. (Eng) degree from the Department of Electrical and Electronic Engineering, University of Stellenbosch, Stellenbosch, South Africa. His current research focuses on the design and optimization of electric traction motors for electric vehicles, including computer-aided design.

Maarten J. Kamper (SM'2008) received the M.Sc. (Eng.) degree in 1987 and the Ph.D. (Eng.) degree in 1996 both from the University of Stellenbosch, Stellenbosch, South Africa. He has been with the academic staff of the Department of Electrical and Electronic Engineering, University of Stellenbosch, since 1989, where he is currently a Professor of electrical machines and drives. His research interests include computer-aided design and control of reluctance, permanent magnet and induction machine drives. Prof. Kamper is a South African National Research Foundation Supported Scientist and a Registered Professional Engineer in South Africa.